Osmotic Gradient-induced Water Permeation across the Sarcolemma of Rabbit Ventricular Myocytes

MIRIK A. SULEYMANIAN and CLIVE MARC BAUMGARTEN

Department of Physiology, Medical College of Virginia, Virginia Commonwealth University, Richmond, Virginia 23298-0551

ABSTRACT The mechanism of water permeation across the sarcolemma was characterized by examining the kinetics and temperature dependence of osmotic swelling and shrinkage of rabbit ventricular myocytes. The magnitude of swelling and the kinetics of swelling and shrinkage were temperature dependent, but the magnitude of shrinkage was very similar at 6°, 22°, and 37°C. Membrane hydraulic conductivity, L_p, was $\sim 1.2 \times 10^{-10}$ liter·N^{-1}·s^{-1} at 22°C, corresponding to an osmotic permeability coefficient, P_f, of 16 μm·s^{-1}, and was independent of the direction of water flux, the magnitude of the imposed osmotic gradient (35–165 mosm/liter), and the initial cell volume. This value of L_p represents an upper limit because the membrane was assumed to be a smooth surface. Based on capacitive membrane area, L_p was 0.7 to 0.9×10^{-10} liter·N^{-1}·s^{-1}. Nevertheless, estimates of L_p in ventricle are 15 to 25 times lower than those in human erythrocytes and are in the range of values reported for protein-free lipid bilayers and biological membranes without functioning water channels (aquaporin). Evaluation of the effect of unstirred layers showed that in the worst case they decrease L_p by ≤2.3%. Analysis of the temperature dependence of L_p indicated that its apparent Arrhenius activation energy, E_a', was 11.7 ± 0.9 kcal/mol between 6° and 22°C and 9.2 ± 0.9 kcal/mol between 22° and 37°C. These values are significantly greater than that typically found for water flow through water-filled pores, ~4 kcal/mol, and are in the range reported for artificial and natural membranes without functioning water channels. Taken together, these data strongly argue that the vast majority of osmotic water flux in ventricular myocytes penetrates the lipid bilayer itself rather than passing through water-filled pores.

INTRODUCTION

Osmotic gradients cause shrinkage and swelling of cardiac muscle, but the permeability of the cardiac sarcolemma to water has never been quantified, and the mechanism of water permeation is unknown. The ability of water to cross membranes depends greatly on the type of cell considered (Dick, 1966; House, 1974; Verkman, 1993). Membranes of many water-transporting epithelia, vascular endothelium, and mammalian erythrocytes (RBCs) are highly permeant, which is a characteristic necessary for transcellular water transport and cell function under conditions of varying osmolarity. In contrast, oocytes, leukocytes, neuronal membranes, and certain epithelia are relatively impermeant.

Recent studies have established that high water permeability results from the expression of aquaporins, a family of specific water channels including CHIP28 (AQP-1) (Agre et al., 1993; Verkman, 1993). For example, mercurials reduce the water permeability of human RBCs by >90% (Macey and Farmer, 1970) and of rabbit RBCs by 98% (Tsai et al., 1991) by inhibiting AQP-1 (Preston et al., 1992; van Hoek and Verkman, 1992). The remaining permeability is thought largely to result from water penetrating the lipid barrier itself (Fettiplace and Haydon, 1980; Finkelstein, 1987). In addition, a small water flow traverses ion channels (Hasegawa et al., 1992) and transporters (Fischbarg et al., 1990).

Based on function and physiological osmotic conditions, one might expect that the cardiac sarcolemma would not need water channels and would have a low water permeability. Nonetheless, AQP-1 mRNA and protein have been identified in heart by in situ hybridization and immunostaining. High levels are found in the vascular endothelium, endocardium, valves, and septa in hearts of fetal and adult rats (Bondy et al., 1993; Hasegawa et al., 1994), and message is said to be "diffusely detectable" in adult animals (Bondy et al.,

Address correspondence to Dr. Clive Marc Baumgarten, Department of Physiology, Medical College of Virginia, Virginia Commonwealth University, Richmond, VA 23298-0551. Fax: (804) 828-7382; E-mail: baumgart@ruby.vcu.edu

 J. GEN. PHYSIOL. © The Rockefeller University Press • 0022-1295/96/04/503/12 $2.00
Volume 107 April 1996 503–514

1993). These data do not distinguish whether AQP-1 is present in muscle or non-muscle cells. More recently, however, immunoreactive AQP-1 was localized to the sarcolemma of isolated rat ventricular myocytes (Zheng et al., 1995). Immunoreactive protein also is found in homogenates of adult rabbit heart (Zheng et al., 1995), but the cellular origin of the material is unknown.

The present study took a functional approach to assessing water permeation in heart and used digital videomicroscopy to characterize the kinetics and temperature dependence of the swelling and shrinkage of ventricular myocytes in response to osmotic gradients. These data permitted calculation of sarcolemmal water permeability, expressed as hydraulic conductivity, L_p. L_p of cardiac sarcolemma was 1.2×10^{-10} liter·$N^{-1} \cdot s^{-1}$ at 22°C using a simple geometric model to estimate the surface-to-volume ratio. If capacitive estimates of membrane area are used instead, L_p was 0.7 to 0.9×10^{-10} liter·N^{-1}·s^{-1}. These values of L_p are 15 to 25 times less than that of mammalian RBCs (Solomon, 1989) and are in the range of protein-free lipid bilayers and liposomes containing cholesterol and biological membranes without functioning water channels (Fettiplace and Haydon, 1980; Finkelstein, 1987). Insight into the mechanism of water permeation in heart was gained from the temperature dependence of the kinetics of swelling and shrinkage. The apparent activation energy, E_a', of L_p was ~10 kcal/mol between 6° and 37°C. This is in the range of values obtained for lipid bilayers, liposomes, and biological membranes without functioning water channels and much higher than the ~4 kcal/mol obtained for water flux through water channels and viscous water flow (Sha'afi and Gary-Bobo, 1973; Macey, 1979; Finkelstein, 1987; Verkman, 1993). Taken together, the low hydraulic conductivity and high activation energy suggest that water channels do not significantly contribute to sarcolemmal water permeability in rabbit ventricular myocytes. The primary route for water crossing cardiac membranes is likely to be directly through the lipid bilayer itself.

A preliminary report of these studies was presented to the Biophysical Society (Suleymanian and Baumgarten, 1994).

MATERIALS AND METHODS

Cell Isolation Procedure

Hearts from rabbits (New Zealand White, 2.5–3 kg) were mounted on a Langendorff apparatus, and ventricular myocytes were isolated by a collagenase-pronase dispersion method (Clemo and Baumgarten, 1991; Clemo et al., 1992). The isolated myocytes were stored in a modified KB solution containing (in millimolar): 132 KOH, 120 glutamic acid, 2.5 KCl, 10 KH_2PO_4, 1.8 $MgSO_4$, 0.5 K_2EGTA, 11 glucose, 10 taurine, 10 HEPES (pH 7.2; 295 mosm/liter). This procedure typically gave ~60% rod-shaped, Ca^{2+}-tolerant, viable cells after transfer to Ca^{2+}-containing Tyrode's solution. Myocytes were used within 6 h of harvesting, and only quiescent cells without membrane blebs were selected for the experiments.

Experimental Solutions

The basic Tyrode's solution contained (in millimolar): 150 NaCl, 5 KCl, 2.5 $CaCl_2$, 1.2 $MgSO_4$, 10 glucose, and 5 HEPES (pH 7.4) and was equilibrated with 100% O_2. Osmotic water movements were studied at a constant ionic strength by replacing 80 mM NaCl with 22.5, 54.5, 96, 125, 160, or 485 mM mannitol. The solution containing 160 mM mannitol was defined as 1T (330 mosm/liter) and was shown to be isotonic with basic Tyrode's solution (Drewnowska and Baumgarten, 1991). The osmolarity of the other bathing solutions ranged from 165 to 660 mosm/liter, 0.5 to 2.0 times that of 1T (i.e., 0.5T to 2T). Osmolarity was routinely verified with a freezing point depression osmometer (Osmette S, Precision Systems, Natick, MA).

Myocytes were placed in a poly-L-lysine–coated, 250-μl, glass-bottomed chamber mounted on a Peltier device and were superfused with bathing solution at ~5 ml/min. Each cell was studied at several osmolarities but only one temperature, 37°, 22°, or 6°C. Modest changes in flow rate were noted on switching to solutions with different mannitol concentrations. In the worst case, an increase from 160 to 485 mM mannitol (1T to 2T) is expected to increase solution viscosity by ~19%. Solution changes were complete ($t_{10\text{–}90\%}$) in 6–8 s, as estimated from the liquid junction potential of a microelectrode placed at the position of the myocytes in the chamber.

Determination of Relative Cell Volume

Videomicroscopy and image analysis methods for measuring cell volume have been described in detail previously (Clemo and Baumgarten, 1991; Clemo et al., 1992). Myocytes were visualized with a TV camera (Dage CCD72; Dage-MTI; Michigan City, IN) coupled to an inverted microscope equipped with Hoffman modulation contrast optics. Images were captured on-line by a frame-grabber. Timing of image acquisition was controlled by custom software written in C and assembly language. To adequately describe the kinetics of volume changes, images were captured every 5 or 10 s for the first 1–2 min after solutions were switched, and at 20- or 30-s intervals thereafter. A combination of commercial (JAVA; Jandel, Corte Madera, CA) and custom (written in ASYST; Keithley, Taunton, MA) programs were used to obtain cell width, length, and the area of the image.

Changes in cell width and thickness on exposure to anisosmotic solutions are proportional (Drewnowska and Baumgarten, 1991). Using each cell as its own control, relative cell volume was calculated as:

$$volume_t/volume_c = (area_t \times width_t)/(area_c \times width_c), \quad (1)$$

where t and c refer to anisosmotic test (e.g., 0.5T) and control (1T) solutions, respectively. These methods provide estimates of relative cell volume that are reproducible to <1%.

For estimating absolute cell volume and membrane surface area, myocytes were assumed to be brick-shaped with equal width and thickness. This corresponds to the results of optical measurements on freshly isolated rabbit ventricular myocytes, which found that the average width and thickness of cells as they happened to settle were not distinguishable, although the ratio of

minor and major axes of the cross-section of individual cells was 0.78 ± 0.05 (Drewnowska and Baumgarten, 1991). A very similar ratio, 0.76, was obtained for fixed rabbit ventricular myocytes (Nassar et al., 1987).

Determination of Hydraulic Conductivity

Hydraulic conductivity, L_p, also called the osmotic permeability coefficient, measures the ability of water to permeate the sarcolemma. Formally, L_p [liter·N^{-1}·s^{-1}; equivalent to 0.01 cm^3·dyn^{-1}·s^{-1} in *cgs* units] relates the water volume flux, J_v [liter·m^{-2}·s^{-1}], to the difference in osmotic pressure across the membrane, $\Pi_i - \Pi_o$ [N·m^{-2}]:

$$J_v = L_p(\Pi_i - \Pi_o). \tag{2}$$

L_p is proportional to the filtration coefficient, P_f [m·s^{-1}]:

$$P_f = RTL_p/\bar{V}_w, \tag{3}$$

where $\bar{V}_w$ is the molar volume of water, R is the gas constant, and T is absolute temperature. $RT/\bar{V}_w$ equals 1.422, 1.359, and 1.288×10^5 N·m·liter^{-1} at 37°, 22°, and 6°C, respectively.

Methods for calculating L_p from the time course of cell volume perturbations have been reviewed in detail by Macey (1979) and Solomon (1989). Two methods were useful for the present experimental paradigm. Both begin with the Kedem–Katchalsky equations coupling solute flux to water flow and assume that $\Pi_o = \Pi_i$ in the steady state and that solute fluxes are negligible. This is a reasonable assumption; we previously showed that rabbit ventricular myocytes behave as perfect osmometers between 0.6T and 2.6T with an osmotically inactive volume fraction of 0.34 (Drewnowska and Baumgarten, 1991), and similar results were obtained in the present studies. The rate of change of relative cell volume, $d\hat{V}_c/dt$, in response to a step change in Π_o is then given by

$$\frac{d\hat{V}_c}{dt} = L_p\frac{A}{V_0}\left[\frac{(1-\hat{V}_b)\Pi_i}{\hat{V}_c - \hat{V}_b} - \Pi_o\right], \tag{4}$$

where A is the sarcolemmal surface area, V_0 is the absolute cell volume at time $t = 0$, $\hat{V}_c$ is the relative cell volume as a function of time, and $\hat{V}_b$ is the osmotically inactive volume fraction. By the assumptions above, Π_i is taken as equal to Π_o before the step, and Π_o refers to the osmotic pressure of the new solution. Integrating and rearranging yields an expression for L_p:

$$L_p\left[\frac{A(\Pi_o)^2}{V_0\Pi_i}\right]t = [1-\hat{V}_b]\left[\ln\frac{\Pi_i - \Pi_o}{\Pi_i - \frac{\hat{V}_c - \hat{V}_b}{1-\hat{V}_b}\Pi_o} - \frac{\Pi_o(\hat{V}_c - 1)}{\Pi_i(1-\hat{V}_b)}\right] \tag{5}$$

A plot of the right side of the equality as a function of time gives a straight line with a slope that is proportional to L_p. This so-called nonlinear method is appropriate to analyze both large (nonlinear) and small perturbations of cell volume.

The second method for calculating L_p is an approximation that is valid only for small perturbations. If the imposed osmotic gradient is small, e.g., ≤50 mosm/liter, Eq. 4 can be simplified, and $d\hat{V}_c/dt$ is given by

$$\frac{d\hat{V}_c}{dt} \simeq \frac{L_pA\Pi_o(\hat{V}_c - \hat{V}_{c,\infty})}{\hat{V}_{c,\infty} - \hat{V}_b}, \tag{6}$$

where $\hat{V}_{c,\infty}$ is the steady-state relative cell volume. In this case, the time course of $\hat{V}_c$ is exponential, and L_p can be calculated from its time constant, τ_w, which reflects water movement:

$$\tau_w = \frac{V_0(1-\hat{V}_b)\Pi_i}{L_pA(\Pi_0)^2} \tag{7}$$

For a 50 mosm/liter osmotic gradient, the error in the estimate of L_p introduced by the simplification is ~3% (Solomon, 1989).

In calculating L_p, it was assumed that membrane surface area, A, did not change from its value in 1T solution; that is, cell swelling and shrinkage were accommodated by membrane unfolding or folding without a change in area. This assumption was verified in separate experiments. Membrane capacitance, measured by a sensitive dual-frequency method similar to that of Rohlicek and Schmid (1994) except implemented in software, was unchanged on switching between 1T, 0.5T, and 2T (Chen, J., Wang, K., and C.M. Baumgarten, unpublished observations). Because sarcolemmal surface area is amplified by folds, caveolae, and T tubules (Stewart and Page, 1978; Levin and Page, 1980), geometric estimates of the surface/volume ratio probably are low by a factor of 1.3 to 1.7. This means that L_p will be overestimated by the same factor (see Discussion). The choice of geometric model has a smaller effect. The surface/volume ratios obtained for cells with square, circular, rectangular, and elliptical cross-sections of the present dimensions are within 15%.

Statistics

Data are reported as the mean ± standard error, except as noted; n represents the number of cells. Fits to Eq. 5 and 7 were carried out cell by cell in ASYST. When multiple comparisons were made, the data were subjected to analysis of variance and either Bonferroni's or Dunn's method for group comparisons, as appropriate (SIGMASTAT, Jandel). The null hypothesis was rejected for $P < 0.05$.

RESULTS

Kinetics and Temperature Dependence of Changes in Cell Volume

Fig. 1 illustrates experiments designed to elucidate the kinetics and temperature dependence of osmotic swelling and shrinkage. First, two control measurements were made 3 min apart in 1T media to ensure that cell volume was stable; then the solution bathing the cell was switched between 1T, 0.5T, and 2T media for 7-min periods at 37° and 22°C (Fig. 1, *A* and *B*) or for 16-min periods at 6°C (Fig. 1 *C*). Cell volume smoothly approached a new steady state after an osmotic challenge, and the swelling or shrinkage was fully reversible. For example, replacing 1T with 0.5T solution at 37°C caused relative cell volume to increase from 1.0 to 1.580 ± 0.017 (n = 12), and volume returned to 1.005 ± 0.011 on switching back to 1T. Myocyte shrinkage also was fully reversible. Volume decreased to 0.677 ± 0.005 (n = 23) in 2T at 37°C, and recovered to 0.995 ± 0.004 on readmitting 1T media. The order of exposure to 0.5T and 2T solutions and the number of solutions tested did not affect the magnitude or kinetics of the

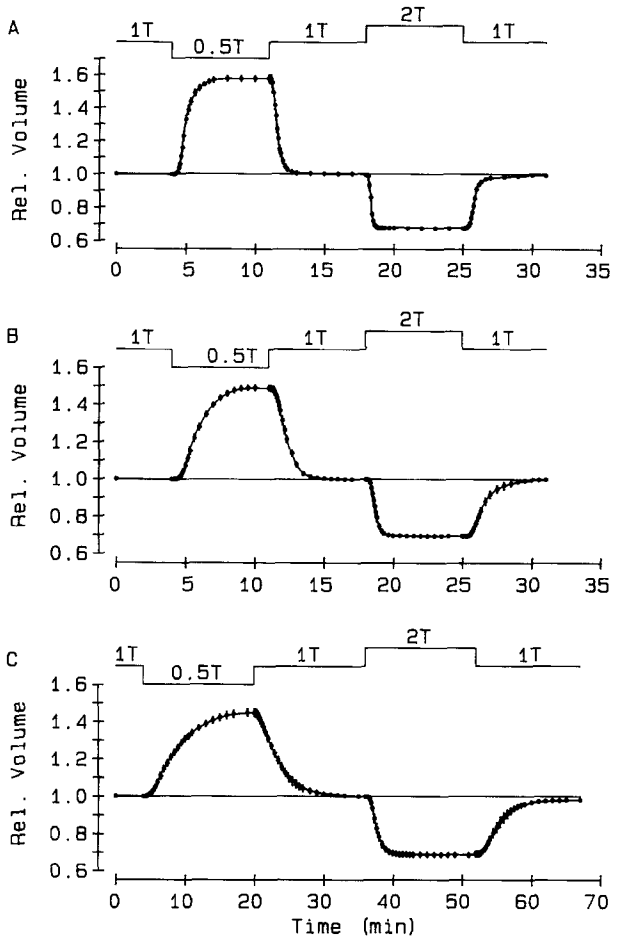

FIGURE 1. Myocyte swelling and shrinkage in 0.5T (165 mosmol/liter) and 2T (660 mosmol/liter) solutions at (*A*) 37°C, (*B*) 22°C, and (*C*) 6°C. Relative volume was measured at 5–60-s intervals. The kinetics of swelling and shrinkage were temperature dependent (time scale changes in panel *C*), and at each temperature, swelling was slower than shrinkage with the same osmotic gradient. The magnitude of swelling also was temperature dependent. Relative cell volume increased in 0.5T from 1.0 to 1.580 ± 0.017 (n = 12), 1.492 ± 0.014 (n = 15), and 1.435 ± 0.020 (n = 12) at 37°, 22°, and 6°C, respectively. In contrast, cell shrinkage in 2T was unaffected by temperature, 0.677 ± 0.005 (n = 23), 0.697 ± 0.005 (n = 16), 0.687 ± 0.012 (n = 7), respectively. Error bars represent mean ± SEM.

volume perturbations. In approximately half of the experiments, myocytes first were exposed to 2T rather than 0.5T solution, and in some experiments, only one anisosmotic solution was applied. These variations were not distinguishable, and all of the experiments were combined.

The effects of temperature on myocyte swelling and shrinkage are more clearly shown in Fig. 2 in which portions of the curves from Fig. 1, *A–C*, are superimposed. The magnitude of swelling on going from 1T to 0.5T significantly decreased on cooling ($P < 0.001$). As noted above, cells swelled to 1.580 at 37°C, but swelled only to 1.492 ± 0.014 (n = 15) and 1.435 ± 0.020 (n = 12) at 22° and 6°C, respectively. That is to say, osmotic swelling at 6°C was 75% of that at 37°C. In contrast, the magnitude of shrinkage on going from 1T to 2T was unaffected by temperature; 0.677 ± 0.005 (n = 23), 0.697 ± 0.005 (n = 16), and 0.687 ± 0.012 (n = 7), at 37°, 22°, and 6°C, respectively. Because osmolyte transport processes are temperature dependent, the simplest explanation for these data is that net transmembrane osmolyte fluxes elicited by osmotic stress do not affect the final volume attained in response to hyperosmotic solutions but may contribute to the volume response under hyposmotic conditions. It should be noted, however, that the volume of a cell was measured at one temperature only for technical reasons. Consequently, these data cannot distinguish whether isosmotic cell volume or the magnitude of the response to osmotic stress was temperature dependent.

The kinetics of osmotic volume changes were characterized by measuring the half-times for swelling and shrinkage (see Table I). Two trends were significant. First, the $t_{1/2}$ was increased approximately fivefold on cooling from 37° to 6°C. For example, $t_{1/2}$ for swelling on switching from 1T to 0.5T slowed from 37.0 ± 2.4 s (n = 12) to 185.0 ± 12.6 s (n = 12). Second, the $t_{1/2}$ for cell swelling was significantly slower than that for cell shrinkage, even when the volume changes were identical. At 37°C, the $t_{1/2}$ was 37.0 ± 2.4 (n = 12) for swelling on switching from 1T to 0.5T and 24.9 ± 1.1 s (n = 12) for shrinkage on switching back.

Hydraulic Conductivity

The time course of an osmotic volume change is complex and is expected to depend on several factors, including the permeability of the sarcolemma to water, the surface/volume ratio, and the initial and final osmolarities (Macey, 1979; Solomon, 1989). To delineate the properties of the sarcolemmal membrane itself, L_p was calculated from the kinetics of cell swelling and shrinkage. Fig. 3 illustrates the analytical methods using data from the swelling of a cell on substituting 0.89T for 1T solution at 22°C. Because the imposed osmotic gradient (35 mosm/liter) and cell swelling (7.9%) were small, both the small perturbation method (see Eq. 7) and the nonlinear method (see Eq. 5) were applied to these data. Except for the first few time points, which were affected by solution mixing, the time course of swelling was well described by an exponential, and τ_w was 64.9 s (Fig. 2 *A*). Fig. 3 *B* uses the same data, but the right side of Eq. 5, denoted $f(V)$, is plotted instead of relative cell volume. The slope of the relationship was 0.00972. The values of L_p calculated from these parameters were in close agreement, 0.87 and 0.88 × 10^{-10} liter·N^{-1}·s^{-1}, respectively.

Both methods were used to analyze all small pertur-

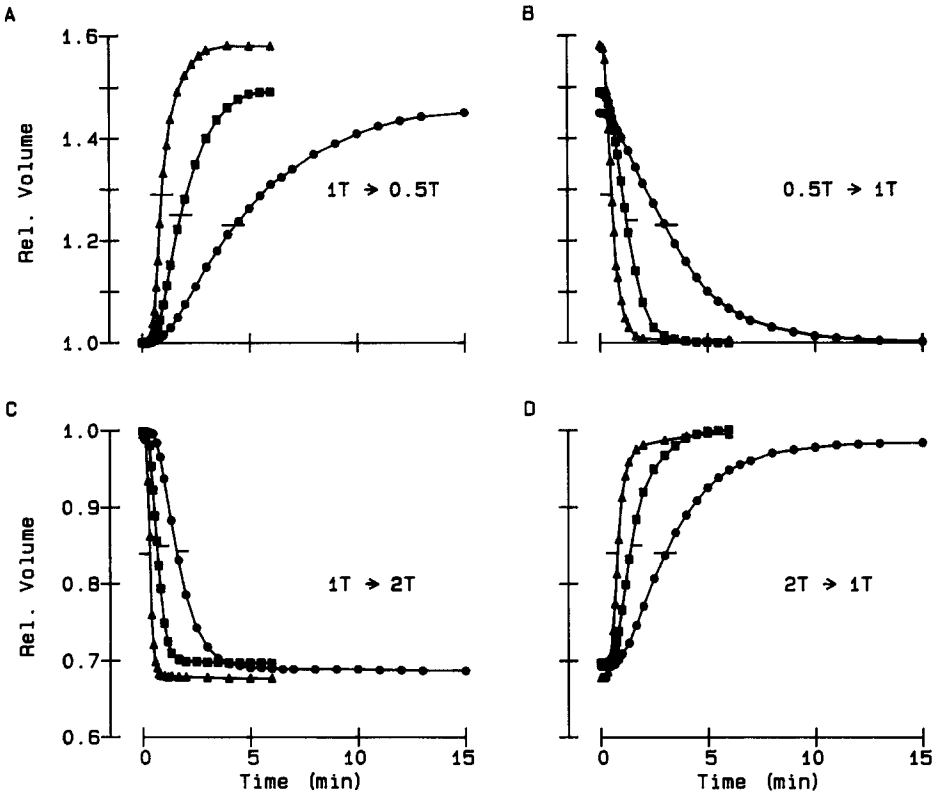

FIGURE 2. Kinetics and magnitude of swelling and shrinkage on switching from (*A*) 1T→0.5T, (*B*) 0.5T→1T, (*C*) 1T→2T, and (*D*) 2T→1T at 37°C (▲), 22°C (■), and 6°C (●). Data from Fig. 1 were superimposed to facilitate comparison. Half-times are denoted by horizontal lines (see Table I). Error bars were omitted for clarity.

bation data sets (n = 52) obtained on switching from 1T to 0.89T and from 0.89T to 1T at 22°C. L_p was 1.24 ± 0.07 × 10^{-10} liter·N^{-1} · s^{-1} by the small perturbation method and 1.26 ± 0.06 × 10^{-10} liter · N^{-1} · s^{-1} by the nonlinear method. These values were statistically indistinguishable in a paired comparison and correspond to a P_f of 17 μm · s^{-1}. This means that the membrane permeability to water in ventricular myocytes is at least 15 times less than that in RBCs at comparable temperatures (Solomon, 1989) and is in the range reported for protein-free artificial lipid bilayers (Fettiplace and Haydon, 1980; Finkelstein, 1987).

L_p also was calculated from the kinetics of myocyte swelling and shrinkage on switching between 1T, 0.5T, and 2T solutions. In this protocol (see Fig. 1), the applied osmotic gradients and volume changes were large, and only the nonlinear method (Fig. 3 *B*; Eq. 5) was appropriate. Fig. 4 illustrates the results of the analysis. L_p decreased on cooling, and the medians at each temperature were significantly different from each other. Because the variance of L_p in each experimental group depended on the mean, the data are presented as box plots indicating the median, 25th percentile, and 75th percentile values. Averaged over all the perturbations, L_p was 2.4 ± 0.1 × 10^{-10} (n = 57), 1.1 ± 0.1 × 10^{-10} (n = 54), and 0.35 ± 0.10 × 10^{-10} (n = 26) liter·N^{-1} · s^{-1} at 37°, 22°, and 6°C, respectively. In contrast to the clear effect of temperature, the L_p's obtained from swelling and shrinkage in a pair of solutions (i.e., 1T→0.5T versus 0.5T→1T and 1T→2T versus 2T→1T) could not be distinguished by these methods, although the values for swelling tended to be slightly greater than those for shrinkage.

TABLE I

Temperature Dependence of the Kinetics of Cell Volume Changes

Osmotic challenge	$t_{1/2}$,s [mean ± sem (n)]		
	37°C	22°C	6°C
1T → 0.5T	37.0 ± 2.4 (12)	70.7 ± 4.0 (15)	185.0 ± 12.6 (12)
0.5T → 1T	24.9 ± 1.1 (12)	50.6 ± 1.9 (15)	165.4 ± 12.9 (12)
1T → 2T	15.1 ± 0.7 (23)	26.5 ± 1.3 (16)	66.4 ± 4.9 (7)
2T → 1T	27.2 ± 1.2 (23)	39.7 ± 1.9 (16)	125.0 ± 11.5 (7)

Apparent Activation Energy of L_p

The apparent activation energy of L_p provides information about the mechanism of water permeation through the sarcolemma. For water traversing a water-filled pore, E_a' is expected to be ~4 kcal·mol^{-1}, reflecting the temperature dependence of the viscosity of water (Sha'afi and Gary-Bobo, 1973; Macey, 1979; Finkelstein, 1987; Verkman, 1993). Fig. 5 shows Arrhenius plots of L_p data for each of the osmotic perturbations. For the four osmotic challenges, E_a' averaged 11.7 ± 0.9 kcal/mol between 6° and 22°C and 9.2 ± 0.9 kcal/mol between 22° and 37°C. The individual esti-

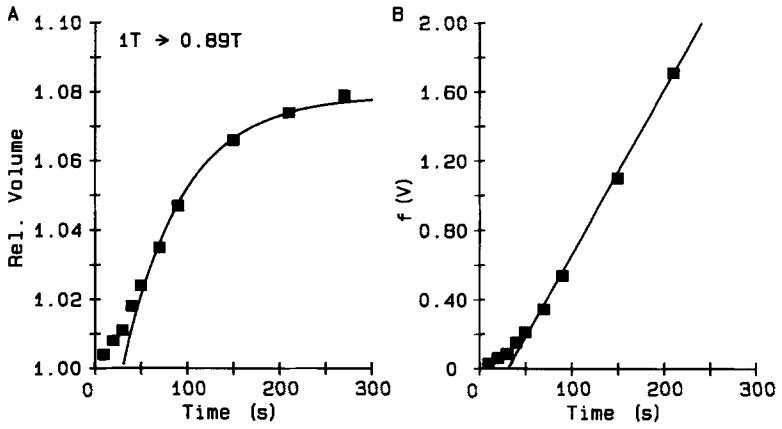

FIGURE 3. Measurement of hydraulic conductivity, L_p, by the (*A*) small perturbation (see Eq. 7) and (*B*) nonlinear (see Eq. 5) methods during swelling of a myocyte on switching from 1T to 0.89T solution. The parameters necessary to calculate L_p, including the osmotically inactive volume, were calculated for each cell for each osmotic step. (*A*) Time course of small volume perturbation fit an exponential; τ_w was 64.9 s. (*B*) For small or large perturbations, plotting $f(V)$, which represents the right hand side of Eq. 5, versus time gives a straight line with a slope equal to $L_p A \Pi_o^2 / V_0 \Pi_i$. Both methods gave nearly identical values for L_p, 0.866 and 0.882×10^{-10} liter · N^{-1} · s^{-1}, respectively, in this example. Least-squares fits were done in ASYST after excluding the first three points to avoid the effect of solution mixing. Time scale was not corrected for the dead time in the perfusion system.

mates ranged from 8 to 13 kcal/mol. These values are significantly greater than those expected for viscous water flow through a water-filled pore and imply that the majority of osmotic water movement occurs by a different mechanism.

Does the Magnitude of the Osmotic Gradient or Initial Cell Volume Affect L_p?

In theory, L_p is a characteristic of the membrane and should be independent of the magnitude and direction of the osmotic gradient, at least for a simple membrane. These predictions were verified using the experimental protocol depicted in Fig. 6 *A*. Myocytes were repeatedly switched between hyposmotic and isosmotic solutions (n = 6). Cell volume increased to 1.083 ± 0.006, 1.160 ± 0.009, 1.300 ± 0.015, and 1.418 ± 0.031 in 0.89T, 0.80T, 0.67T, and 0.57T solutions, respectively, and each time cell volume returned to its initial value in 1T. Fig. 6 *B* shows the relationship between L_p and the osmotic gradient (35 to 142 mosm/liter) for these eight interventions. No statistically significant differences in L_p were detected between any of the groups, although an F-ratio test suggested an overall effect of treatment group (P = 0.0233). When analyzed by the direction of the osmotic gradient, the L_p for swelling,

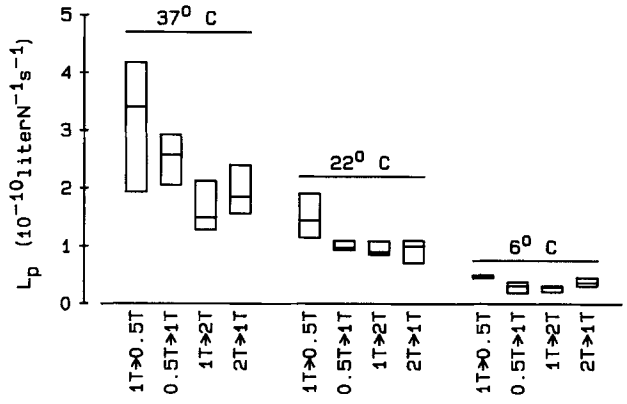

FIGURE 4. Temperature dependence of L_p measured on switching between 1T and 0.5T and between 1T and 2T solutions. Because the variance of L_p depended on the mean, data were analyzed by a Kruskal–Wallis ANOVA on ranks, and box plots illustrate the 25th, 50th, and 75th percentile. Although the effect of temperature was significant ($P < 0.001$), L_p's for osmotic perturbations at the same temperature were not distinguishable in pairwise comparisons (Dunn's method), and the overall effect of the osmotic gradient was not significant (F-ratio test, P = 0.1755).

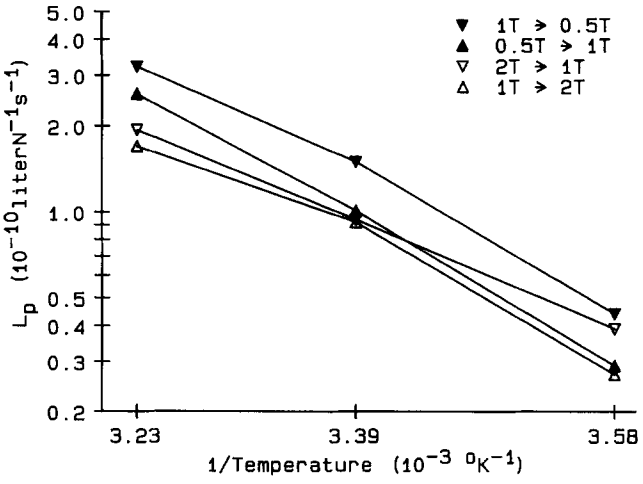

FIGURE 5. Arrhenius plot of L_p on switching from 1T to 0.5T (▼), 0.5T to 1T (▲), 1T to 2T (△), and 2T to 1T (▽). Apparent activation energy, E_a', was calculated from the mean L_p for each condition and was 11.7 ± 0.9 kcal/mol between 6° and 22°C and 9.2 ± 0.9 kcal/mol between 22° and 37°C (n = 4 osmotic steps). E_a' was 11.2 ± 0.3 and 9.2 ± 1.3 kcal/mol, if median L_p's were used instead of means. These values of E_a' are typical of water movement through lipid bilayers and membranes without functioning water channels and are significantly greater than the ~4 kcal/mol expected for osmosis through water-filled pores.

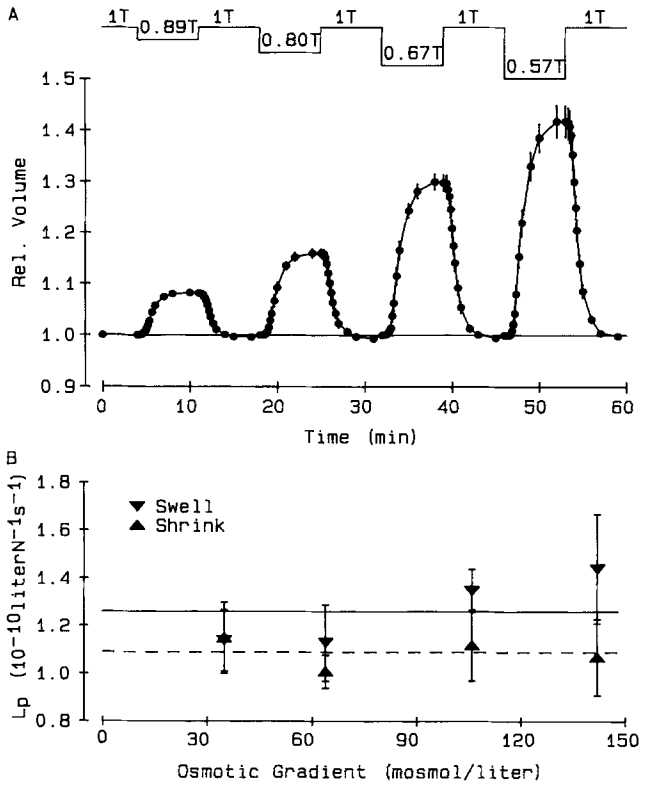

FIGURE 6. L_p was independent of the magnitude and direction of the osmotic gradient. (*A*) Kinetics of volume changes on switching between 1T and 0.89T, 0.80T, 0.67T, or 0.57T solutions at 22°C. Relative cell volume returned to its initial value in isosmotic solution before each hyposmotic challenge; $n = 6$. (*B*) L_p was calculated during swelling (▼) and shrinkage (▲) from data in *A* by the nonlinear method and is plotted as a function of the imposed osmotic gradient. An overall significant effect of treatment group (osmotic gradient) was detected by a repeated measures ANOVA and F-ratio test ($P = 0.0233$), but no significant differences between any of the treatment groups were found in pairwise comparisons (Bonferroni method). The highest value of L_p was obtained with the largest gradient. In contrast, L_p should be inversely related to the magnitude of the gradient if unstirred layer effects are important. Overall, L_p for swelling, $1.26 \pm 0.08 \times 10^{-10}$ liter · N^{-1} · s^{-1} (solid line) was not significantly different from that for shrinkage, $1.09 \pm 0.07 \times 10^{-10}$ liter · N^{-1} · s^{-1} (dashed line).

$1.26 \pm 0.08 \times 10^{-10}$ liter · N^{-1} · s^{-1}, was statistically indistinguishable from that for shrinkage, $1.09 \pm 0.07 \times 10^{-10}$ liter·N^{-1}·s^{-1}.

Another approach for examining these issues is shown in Fig. 7 *A*. Cells were exposed to the same series of hyperosmotic solutions as before, except they were not returned to 1T solution until the end of the experiment. In this case, the imposed osmotic gradients are similar to each other, but the initial cell volumes and Π_i differ. The calculated values of L_p are plotted as a function of initial cell volume in Fig. 7 *B*. No significant differences were identified between any of the groups, and the overall average L_p for swelling, $1.34 \pm 0.11 \times 10^{-10}$ liter·N^{-1}·s^{-1} (solid line), was quite similar to that for shrinkage, $1.26 \pm 0.10 \times 10^{-10}$ liter·N^{-1}·s^{-1} (dashed line). Taken together, these data indicate that the measured value of L_p is independent of the magnitude and direction of the osmotic gradient and the initial cell volume.

Compensatory Volume Regulation

A wide variety of cells exhibit a regulatory volume decrease (RVD) or regulatory volume increase (RVI) in response to osmotic stress (Hoffmann and Simonsen, 1989; McCarthy and O'Neil, 1992; Hallows and Knauf, 1994). Cells initially swell or shrink, and then cell volume partially or fully recovers as a result of activation of compensatory ion transport mechanisms. Previous studies on rabbit cardiac myocytes (e.g., Drewnowska

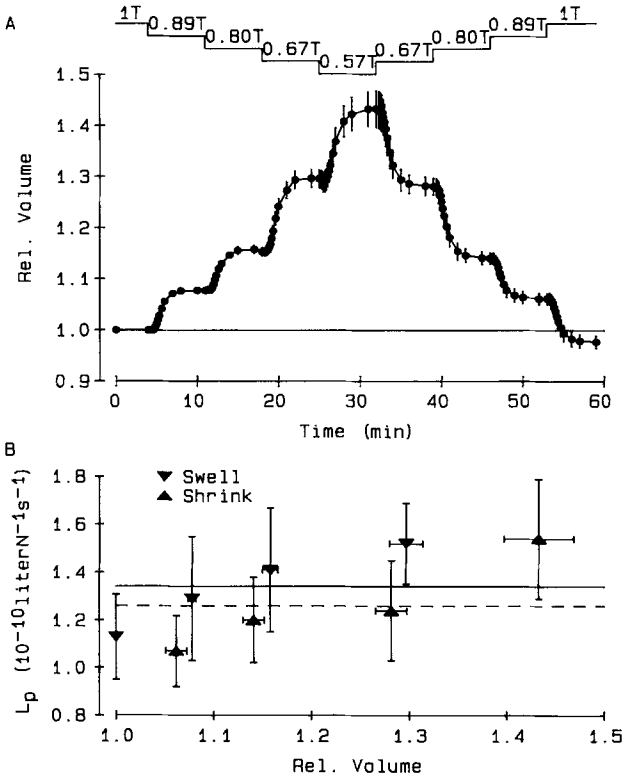

FIGURE 7. L_p was independent of initial osmolarity and cell volume. (*A*) Kinetics of volume changes on switching from 1T to a series of successively more hypotonic solutions (0.89T, 0.80T, 0.67T, 0.57T) and then back again at 22°C; $n = 5$. (*B*) L_p was calculated during swelling (▼) and shrinkage (▲) from data in *A* by the nonlinear method and is plotted as a function of initial cell volume. Overall effect of treatment group (initial osmolarity) approached significance by a repeated measures ANOVA and F-ratio test ($P = 0.0586$), but no significant differences between any of the treatment groups were found in pairwise comparisons (Bonferroni method). Error bars represent ± 1 SEM for both L_p and initial cell volume. Overall, L_p for swelling, $1.34 \pm 0.11 \times 10^{-10}$ liter · N^{-1} · s^{-1} (solid line) was not significantly different from that for shrinkage, $1.26 \pm 0.10 \times 10^{-10}$ liter · N^{-1} · s^{-1} (dashed line).

and Baumgarten, 1991) did not find evidence for RVDs or RVIs when myocytes were exposed to solutions ranging from 0.6T to 1.8T. In contrast, cultured embryonic chick heart undergoes a significant RVD on swelling (Rasmusson et al., 1993). In the present study, RVDs and RVIs are absent in 0.5T and 2T solution in Fig. 1. This was not always the case, however. Fig. 8 shows that most rabbit ventricular myocytes undergo a classic RVD in 0.5T solution at 37°C, but still do not exhibit a RVI in 2T solution. In these experiments relative cell volume increased to a maximum of 1.412 ± 0.028 (n = 6) more than 2 min after switching to 0.5T solution and then decreased to 1.316 ± 0.024 after 6 min. An additional eight less-complete experiments showed similar results. The compensatory response illustrated in Fig. 8, although incomplete, amounted to a 23% decrease of volume from its peak level in those cells, but a 46% decrease from the level attained in cells without an RVD, 1.580 ± 0.017 (n = 12) (Fig. 1 *A*). On returning myocytes to 1T solution, the volume of cells exhibiting an RVD decreased to 0.940 ± 0.010, a value significantly less than 1.0. However, the undershoot during recovery was far less than the RVD during swelling, implying that osmolytes were not permanently lost. In contrast to the regulatory response observed on swelling in hyposmotic solution, no RVI was observed during hyperosmotic shrinkage. Relative to the initial volume in 1T, volume smoothly decreased to 0.655 ± 0.016 in 2T solution; this is equivalent to a volume of 0.697 ± 0.017 relative to the 1T volume immediately before cell shrinkage. Thus, despite exhibiting a RVD, cell shrinkage was almost identical to that shown in Fig. 1 *A*, 0.677 ± 0.005. In addition to these experiments at 37°C, RVDs were noted on switching to 0.5T media in 3 of 20 cells at 22°C but never were observed at 6°C. Also, RVDs never were observed during smaller osmotic perturbations, such as those shown in Fig. 6 *A* (e.g., 1T→0.59T) or Fig. 7 *A*. The mechanism underlying RVDs during strong osmotic stress was not investigated further.

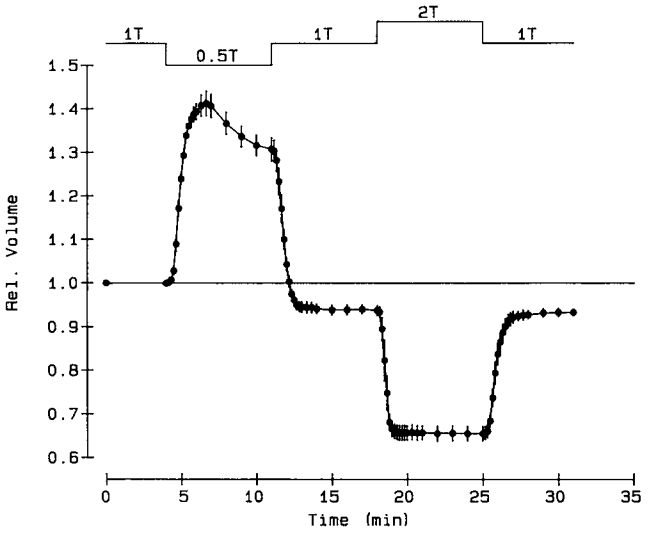

FIGURE 8. Myocytes can exhibit a regulatory volume decrease on switching from 1T to 0.5T solution at 37°C. Relative cell volume in 6 cells increased to a maximum of 1.412 ± 0.028 and then decreased to 1.316 ± 0.024 after 6 min in 0.5T solution (cf., Fig. 1 *A*). On returning to 1T solution, cell volume decreased to 0.940 ± 0.010, significantly less than its initial value. In contrast, a regulatory volume increase was not observed in 2T solution.

DISCUSSION

These experiments demonstrate for the first time that the L_p of ventricular myocytes is low. L_p was ~1.2 × 10^{-10} liter · N^{-1} · s^{-1} at 22°C, corresponding to a P_f of 16 μm · s^{-1}. These values represent upper limits, however, because the geometric model used to estimate the surface/volume ratio of ventricular myocytes assumed a smooth surface membrane. Based on capacitive membrane area, L_p was 0.7 to 0.9 × 10^{-10} liter · N^{-1} · s^{-1} (see infra). Estimates of L_p in ventricle are 15 to 25 times lower than those in human RBCs, which average 18 × 10^{-10} liter · N^{-1} · s^{-1} (Solomon, 1989) and are in the range of values reported for protein-free lipid bilayers and liposomes (Fettiplace and Haydon, 1980; Finkelstein, 1987). Analysis of the temperature dependence of L_p indicated that its E_a' was ~10 kcal/mol. This value is greater than expected for water flow through water-filled pores (Sha'afi and Gary-Bobo, 1973; Macey, 1979; Finkelstein, 1987; Verkman, 1993) and implies that the majority of osmotic water movement in ventricular myocytes is through the membrane bilayer instead of through water-filled pores.

Sources of Error in the Calculation of L_p

The calculated value of L_p is inversely proportional to the surface/volume ratio of the cell and therefore depends on the assumed geometric model. Ignoring the ends, smooth circular and square cross-sections both give surface/volume ratios of 0.174 $\mu m^2/\mu m^3$ for a typical 23-μm-wide cell. If rectangular or ellipsoidal cross-sections are assumed instead, the surface/volume ratios are 0.198 and 0.200 $\mu m^2/\mu m^3$, respectively (minor/major axis = 0.78; Drewnowska and Baumgarten, 1991), and the calculated values of L_p need to be reduced by ~13%. Surface/volume ratios for smooth shapes are certainly too low, however, because sarcolemmal folds and invagination are ignored. By stereological analysis, including T tubules as a component of surface membrane, surface/volume ratio is 0.59 to 0.66 $\mu m^2/\mu m^3$ (right papillary muscle, 2.5–3 kg rabbits; Stewart and Page, 1978) after correction for caveolae (Levin and Page, 1980). If these figures are accepted, the calculated L_p needs to be reduced by a factor of 3.4

to 3.8. On the other hand, surface/volume ratios in fixed material may be erroneously high because of specimen shrinkage. The cell diameter obtained by Stewart and Page (1978) was 13–15 μm, much less than the 21–25 μm reported for unfixed isolated rabbit myocytes (e.g., Drewnowska and Baumgarten, 1991; Clemo et al., 1992).

Perhaps a better method for arriving at the surface/volume ratio is to use membrane capacitance (C_m) to estimate surface area assuming a specific membrane capacitance of 1 μF/cm^2 and the geometric method to estimate volume. C_m was not measured in the same cells used to measure volume to avoid the possibility that fluid and solute flux between the cell and pipette would confound the analysis of cell swelling and shrinkage. In parallel experiments, C_m was 164 ± 8 pF (n = 40) in 1T solution. For an exemplar 23-μm by 135-μm cell, this gives surface/volume ratios of 0.23 and 0.29 μm^2/μm^3 for cells with square and circular cross-sections, respectively. These ratios are 1.3 and 1.7 times greater than that assumed in the standard calculation of L_p, and it is likely that L_p is overestimated by the same factor.

Unstirred layers are another potential source of error in the calculation of L_p, although it is important to note that their effect on pressure-driven flow and osmotic coefficients is much less than on diffusional permeability, P_d (House, 1974; Barry and Diamond, 1984; Finkelstein, 1987). Convective water flow sweeps solute toward the membrane on the side with lower osmolarity and away from the membrane on the other side. As long as convection of solute is faster than its diffusion, this acts to reduce the magnitude of the osmotic gradient at the membrane surface and results in underestimation of L_p for the membrane itself. The error can be calculated as

$$L_{p(obs)} = L_{p(memb)} \exp(-J_v \delta / D), \quad (8)$$

where $L_{p(obs)}$ and $L_{p(memb)}$ are the observed and true membrane L_p, δ is the thickness of the unstirred layer, and D is the diffusion coefficient of the osmolytes (Finkelstein, 1987). To evaluate this relationship for the present experiments, J_v was calculated from the time course of relative cell volume (Fig. 1) and the surface/volume ratio, 0.174 μm^2/μm^3, of a cell with a smooth circular or square cross-section. The extracellular osmolytes primarily are NaCl (D_{25} = 1.611 × 10^{-5} cm^2·s^{-1}) and mannitol (D_{25} = 0.682 × 10^{-5} cm^2 · s^{-1}). D was taken as a weighted average based on the concentrations of NaCl and mannitol in 0.5T, 1T, and 2T solutions and was corrected for solution temperature and viscosity using the Stokes–Einstein relationship. Over 6° to 37°C, the values adopted for D ranged from 0.401 to 0.949 × 10^{-5} cm·s^{-1} in 2T, 0.600 to 1.418 × 10^{-5} cm · s^{-1} in 1T, and 0.904 to 2.14 × 10^{-5} cm · s^{-1} in 0.5T. Finally, the unstirred layer thickness, δ, can be estimated as $\sqrt{Dt}$, where t is the time for concentration at the membrane to reach ~90% of its final value (Barry and Diamond, 1984). The time course of electrode junction potential (see Methods) indicates t is <8 s; this means δ is <97 μm. On the other hand, analysis of L_p (e.g., Fig. 3) suggests t may be as much as 30 s, which gives 169 μm for δ. Accepting the higher estimate of δ, the worst case error in L_p was 0.7% at 6°C, 1.1% at 22°C, and 2.3% at 37°C. These errors occur at the time of maximum J_v during shrinkage on switching from 1T to 2T. Because J_v is smaller both at other times during shrinkage in 2T and during other osmotic perturbations, even smaller errors are expected overall.

To validate these estimates, we also calculated δ from hydrodynamic theory (Fischbarg et al., 1993). This approach takes into account the average linear fluid velocity (ϑ; 1.04 cm·s^{-1}), the width of the perfusion path (w; 0.4 cm), the kinematic viscosity (υ; ~1.009, 1.079, and 1.286 cm^2 · s^{-1} for 0.5T, 1T and 2T at 25°C) and D. The Reynolds number (Re) is defined as

$$\mathrm{Re} = \vartheta w / \upsilon, \quad (9)$$

and then the diffusion boundary layer thickness can be calculated as

$$\delta = w(\mathrm{Re}^{-1/2})\,(D/\upsilon)^{1/3}. \quad (10)$$

For 0.5T, 1T, and 2T solutions, the hydrodynamic approach gave values of 56–71 μm for the thickness of the unstirred layer and suggests that the worst case error in L_p is <1%. Differences in the estimates of δ are likely to arise from the fact that t in the $\sqrt{Dt}$ method is the time for diffusion through the unstirred layer, but our values for t represent the sum of chamber mixing time and diffusion through the unstirred layer.

Experimental evidence also argues that unstirred layer effects were small. If the unstirred layers were an important barrier, the observed L_p should have increased as the imposed osmotic gradient was made smaller, reducing J_v and the convection of solutes (see Eq. 8). To the contrary, L_p was independent of the size of the applied osmotic gradient during cell shrinkage and, if anything, had an osmotic gradient-dependence opposite to expectations during cell swelling (see Fig. 6 *B*). The same conclusion is reached by considering L_p during a single osmotic transient. The slopes of plots of $f(V)$ versus time, which are proportional to L_p, remained constant as myocytes approached osmotic equilibrium and J_v decreased (Fig. 3 *B*). This implies that the varying bulk flow during an osmotic step did not detectably alter the estimate of L_p. Alternatively, it might be argued that L_p was independent of the osmotic gradient because the rate-limiting barrier was the unstirred layer rather than the membrane, even with the smallest applied gradient in these experiments, 35

mosm/liter. If this argument were correct, the E_a' of L_p should have been ~4 kcal/mol (see infra). In fact, E_a' was significantly greater.

Mechanism of Water Permeation

The apparent activation energy of L_p is diagnostic of the mechanism by which water traverses the membrane (Sha'afi and Gary-Bobo, 1973; Macey, 1979; Finkelstein, 1987; Verkman, 1993). Examples from the literature are given in Table II. Osmosis in tissues expressing endogenous water-filled pores (e.g., mammalian RBCs, proximal tubule basolateral membranes) and liposomes reconstituted with AQP-1 exhibits only a modest temperature dependence with an E_a' of ~4 kcal/mol. This low E_a' arises from the temperature dependence of the viscosity of water. On the other hand, the E_a' for water movement through artificial lipid bilayers, liposomes, and natural membranes without aquaporins (e.g., chicken RBCs, intestinal brush border) or membranes in which aquaporins have been blocked by mercurials (e.g., human RBCs, proximal tubule basolateral membrane) typically is ~10–15 kcal/mol, reflecting the temperature dependence of lipid interactions.

E_a' was 11.7 ± 0.9 kcal/mol between 6° and 22°C and 9.2 ± 0.9 kcal/mol between 22° and 37°C in the present study. These high values for E_a', coupled with a low L_p, strongly argue that most osmotic water flow traverses the cardiac sarcolemma by penetrating the lipid bilayer rather than by passing through water-filled pores. Nevertheless, the possibility that a small fraction of water flux is mediated by aquaporins, ion channels, or transporters cannot be excluded. The observed L_p and E_a' then would depend in a weighted manner on the properties of each of the pathways (Sha'afi and Gary-Bobo, 1973).

The conclusion that water channels do not significantly contribute to osmosis in cardiac myocytes is based on a functional analysis and may seem at odds with the recent report that immunoreactive AQP-1 is present in the sarcolemma of rat ventricular myocytes (Zheng et al., 1995). Even unambiguous identification of AQP-1 in the sarcolemma does not establish the role of water-filled pores in myocyte function, however. The problem is that each AQP-1 monomer imparts a P_f of only $\sim 1.1 \times 10^{-15}$ m·s^{-1} (van Hoek and Verkman, 1992; Zeidel et al., 1992), equivalent to an L_p of $\sim 8 \times 10^{-21}$ liter·N^{-1}·s^{-1}. This means that AQP-1 at a density of 10 monomers·μm^{-2} would account for <7% of the measured sarcolemmal L_p. Consequently, AQP-1 or other aquaporins might be detected at a molecular level by highly sensitive techniques without significantly adding to sarcolemmal water permeability.

On the other hand, it is possible that enzymes used to isolate myocytes inactivated the water channels. The best argument against this is that water channels continue to function in other cells treated with various proteases, e.g., freshly suspended cultured lung alveolar epithelia and AQP1-transfected CHO cells (Ma et al., 1993; Folkesson et al., 1994). Nevertheless, we cannot definitively rule out the possibility that enzyme treatment or other steps in the isolation procedure affected water channel function.

The detailed mechanism of osmotic water movement through the lipid bilayers remains uncertain. Most commonly, a partition-diffusion mechanism is invoked in which the hydrophobic membrane core is held to be rate limiting (Fettiplace and Haydon, 1980; Deamer and Bramhall, 1986; Finkelstein, 1987). Water is said to dissolve in the lipid and diffuse down its concentration gradient. A recent transient defect model (Haines, 1994) proposes instead that lateral movement of head groups is rate limiting, and that water passes through the hydrophobic core tucked into *gauche-trans-gauche* kinks, which are known to propagate rapidly down acyl chains. Additional support for this model comes from studies showing addition of cardiolipin to phosphatidylcholine liposomes decreases L_p without a change in bilayer fluidity by stabilizing head group interactions (Shibata et al., 1994). Reasonable agreement with observed permeability values can be obtained by both partition-diffusion and transient defect models. Both models predict that increased temperature, via decreased microviscosity of the hydrophobic core or increased rate of lateral diffusion of phospholipids, respectively, will increase water permeability as found in the present experiments.

TABLE II

Hydraulic Conductivity and Its Apparent Activation Energy

Tissue	L_p (10^{-10}liter · N^{-1} · s^{-1})	E_a' (kcal/mol)
Ventricle, rabbit	1.2[a]	9.2–11.7[a]
RBC, human	18.0[b]	3.9[c]
RBC, beef	18.2[c]	4.0[c]
RBC, dog	23.0[d]	4.3[e]
Proximal tubule BLM, rabbit	21.9[f]	2.5[f]
Intestinal brush border, rat	0.9[g]	9.8[g]
RBC, chicken	0.6[c]	11.4[c]
RBC, human + PCMBS	1.3[h]	11.6[h]
BLM, proximal tubule, rabbit + Hg	4.4[f]	8.2[f]
PC bilayer	1.6[i]	13[i]
PC/Chol bilayer	0.4[j]	12.7[k]
Liposomes	1.9[l]	16.0[l]
Liposomes + AQP-1	30.8[l]	3.1[l]
Viscous water flow	—	4.2[c]

RBC, red blood cell; BLV, basolateral membrane vesicle; PCMBS, *p*-chloromercuribenzene sulfonate; PC, phosphatidylcholine, Chol, cholesterol; [a] Present study; [b] Solomon, 1989; [c] Farmer and Macey, 1970; [d] Rich et al., 1968; [e] Vieira et al., 1970; [f] Verkman and Ives, 1986; [g] Worman and Field, 1985; [h] Moura et al., 1984; [i] Graziani and Livne, 1972; [j] Fettiplace, 1978; [k] Price and Thompson, 1969; [l] Zeidel et al., 1992.

Physiological Implications

Only a few studies have considered osmotic water permeability in any type of muscle. The most detailed analysis was by Sorenson (1971), who examined skeletal muscle fibers from a marine crab (*Chionoecetes bairdi*). He reported L_p was $\sim 38 \times 10^{-10}$ liter·N^{-1}·s^{-1} with osmotic gradients $\leq$32 mosm/liter at 10°C, an L_p 100-fold greater than the 0.35×10^{-10} liter·N^{-1}·s^{-1} obtained in ventricle at 6°C. Because L_p was referred to the apparent surface area assuming a smooth elliptical model, some of this large difference is likely to reflect underestimation of surface area. The L_p of crab fibers decreased to 7.6×10^{-10} liter·N^{-1}·s^{-1} when a greater osmotic gradient (86 mosm/liter) was applied, perhaps because of unstirred layers. In the older literature, values of 16.9, 9.5, and 5.0×10^{-10} liter·N^{-1}·s^{-1} were claimed for frog (Hodgkin and Horowicz, 1959; Zadunaisky et al., 1963) and crayfish skeletal muscle (Reuben et al., 1964), respectively, but full methodological details were not provided. More recently, Berman et al. (1993) calculated an L_p of 1.1×10^{-10} liter·N^{-1}·s^{-1} for giant barnacle skeletal muscle. The agreement with cardiac values is likely to be fortuitous, however. As recognized by the authors, the remarkably extensive and complex invagination of the barnacle sarcolemma will lead to a very serious overestimation of L_p when the apparent surface area of a cylinder is assumed. On the other hand, L_p is likely to be seriously underestimated because the effects of unstirred layers are favored by the large diameter of barnacle muscle cells, the tortuosity of membrane invagination, and the large osmotic gradients applied, 450–2000 mosm/liter.

Because cardiac muscle normally does not transport water, the low L_p and absence of a significant water flux through water channels may not be surprising. Nevertheless, the permeability of cardiac membranes to water is critically important in several situations. For example, low L_p may serve to protect the heart from transient disturbances in serum osmolarity such as that induced by the injection of hyperosmotic radiopaque contrast medium into the coronary arteries. L_p also may be critically important during ischemia and reperfusion. It is well known that ischemia and reperfusion result in rapid cell swelling and cell death, if injury is severe (Reimer and Jennings, 1992). Ischemic metabolites, including lysophospholipids (Hazen and Gross, 1992) and long-chain acyl carnitines (Corr et al., 1995), accumulate in the sarcolemma during ischemia and increase membrane fluidity. It is appealing to speculate that accumulation of these metabolites increases L_p and thereby exacerbates both the rapidity of cell swelling and the extent of ensuing cell injury.

We thank Jude Maghirang for programming and technical assistance, Ray Caldwell for participating in the measurement of membrane capacitance, and Dr. Joseph J. Feher for thoughtful and productive discussions.

This work was supported by the National Heart, Lung and Blood Institute grant HL-46764.

Original version received 3 August 1995 and accepted version received 18 December 1995.

REFERENCES

Agre, P., G.M. Preston, B.L. Smith, J.S. Jung, S. Raina, C. Moon, W.B. Guggino, and S. Nielsen. 1993. Aquaporin CHIP: the archetypal molecular water channel. *Am. J. Physiol.* 265:F463–F476.

Barry, P.H., and J.M. Diamond. 1984. Effects of unstirred layers on membrane phenomena. *Physiol. Rev.* 64:763–873.

Berman, D.M., C. Peña-Rasgado, M. Holmgren, P. Hawkins, and H. Rasgado-Flores. 1993. External Ca effect on water permeability, regulatory volume decrease, and extracellular space in barnacle muscle cells. *Am. J. Physiol.* 265:C1128–C1137.

Bondy, C., E. Chin, B.L. Smith, G.M. Preston, and P. Agre. 1993. Developmental gene expression and tissue distribution of the CHIP28 water-channel protein. *Proc. Natl. Acad. Sci. USA.* 90: 4500–4504.

Clemo, H.F., and C.M. Baumgarten. 1991. Atrial natriuretic factor decreases cell volume of rabbit atrial and ventricular myocytes. *Am. J. Physiol.* 260:C681–C690.

Clemo, H.F., J.J. Feher, and C.M. Baumgarten. 1992. Modulation of rabbit ventricular cell volume and $Na^+/K^+/2Cl^-$ cotransport by cGMP and atrial natriuretic factor. *J. Gen. Physiol.* 100:89–114.

Corr, P.B., J. McHowat, G-X. Yan, and K.A. Yamada. 1995. Lipid-derived amphiphiles and their contribution to arrhythmogenesis during ischemia. *In* Physiology and Pathophysiology of the Heart. 3rd ed. N. Sperelakis, editor. Kluwer Academic Publishers, Boston. 527–545.

Deamer, D.W., and J. Bramhall. 1986. Permeability of lipid bilayers to water and ionic solutes. *Chem. Phys. Lipids.* 40:167–188.

Dick, D.A.T. 1966. Cell Water. Butterworths, Washington, DC. 90–92.

Drewnowska, K., and C.M. Baumgarten. 1991. Regulation of cellular volume in rabbit ventricular myocytes: Bumetanide, chlorothiazide, and ouabain. *Am. J. Physiol.* 260:C122–C131.

Farmer, R.E.I., and R.I. Macey. 1970. Perturbation of red cell volume: rectification of osmotic flow. *Biochim. Biophys. Acta.* 196:53–65.

Fettiplace, R. 1978. The influence of the lipid on the water permeability of artificial membranes. *Biochim. Biophys. Acta.* 513:1–10.

Fettiplace, R., and D.A. Haydon. 1980. Water permeability of lipid membranes. *Physiol. Rev.* 60:510–550.

Finkelstein, A. 1987. Water Movement through Lipid Bilayers, Pores, and Plasma Membranes: Theory and Reality. John Wiley and Sons, New York. 38–41, 158–159, 166–184.

Fischbarg, J., J. Li, K. Kuang, M. Echevarría, and P. Iserovich. 1993. Determination of volume and water permeability of platted cells from measurements of light scattering. *Am. J. Physiol.* 265:C1412–C1423.

Fischbarg, J., K. Kuang, J.C. Vera, S. Arant, S.C. Silverstein, J. Loike, and O.M. Rosen. 1990. Glucose transporters serve as water channels. *Proc. Natl. Acad. Sci. USA.* 87:3244–3247.

Folkesson, H.G., M.A. Matthay, H. Hasegawa, F. Kheradmand, and A.S. Verkman. 1994. Transcellular water transport in lung alveolar epithelium through mercury-sensitive water channels. *Proc. Natl. Acad. Sci. USA.* 91:4970–4974.

Graziani, Y., and A. Livne. 1972. Water permeability of bilayer lipid membranes. Sterol-lipid interaction. *J. Membr. Biol.* 7:275–284.

Haines, T.H. 1994. Water transport across biological membranes. *FEBS (Fed. Eur. Biochem. Soc.) Lett.* 346:115–122.

Hallows, K.R., and P.A. Knauf. 1994. Principles of cell volume regulation. *In* Cellular and Molecular Physiology of Cell Volume Regulation. K. Strange, editor. CRC Press, Boca Raton, FL. 3–29.

Hasegawa, H., S.C. Lian, W.E. Finkbeiner, and A.S. Verkman. 1994. Extrarenal tissue distribution of CHIP28 water channels by in situ hybridization and antibody staining. *Am. J. Physiol.* 266:C893–C903.

Hasegawa, H., W. Skach, O. Baker, M.C. Calayag, V. Lingappa, and A.S. Verkman. 1992. A multifunctional aqueous channel formed by CFTR. *Science (Wash. DC).* 258:1477–1479.

Hazen, S.L., and R.W. Gross. 1992. Principles of membrane biochemistry and their application to the pathophysiology of cardiovascular disease. *In* The Heart and Cardiovascular System. 2nd ed. H.A. Fozzard, E. Haber, R.B. Jennings, A.M. Katz, and H.E. Morgan, editors. Raven Press, New York. 839–860.

Hodgkin, A.L., and P. Horowicz. 1959. The influence of potassium and chloride ions on the membrane potential of single muscle fibers. *J. Physiol.* 148:127–160.

Hoffmann, E.K., and L.O. Simonsen. 1989. Membrane mechanisms in volume and pH regulation in vertebrate cells. *Physiol. Rev.* 69: 315–382.

House, C.R. 1974. Water Transport in Cells and Tissues. Edward Arnold Publishers, London, 101–113, 165, 323–324.

Levin, K.R., and E. Page. 1980. Quantitative studies on plasmalemmal folds and caveolae of rabbit ventricular myocardial cells. *Circ. Res.* 46:244–255.

Nassar, R., M.C. Reedy, and P.A.W. Anderson. 1987. Developmental changes in the ultrastructure and sarcomere shortening of the isolated rabbit ventricular myocyte. *Circ. Res.* 61:465–483.

Ma, T., A. Frigeri, S.-T. Tsai, J.-M. Verbavatz, and A.S. Verkman. 1993. Localization and functional analysis of CHIP28k water channels in stably transfected Chinese hamster ovary cells. *J. Biol. Chem.* 268:22756–22764.

Macey, R.I. 1979. Transport of water and nonelectrolytes across red cell membranes. *In* Membrane Transport in Biology. Vol 2. G. Giebisch, D.C. Tosteson, and H.H. Ussing, editors. Springer-Verlag, Berlin. 1–57.

Macey, R.I., and R.E.L. Farmer. 1970. Inhibition of water and solute permeability in human red blood cells. *Biochim. Biophys. Acta.* 211:104–106.

McCarthy, N.A., and R.G. O'Neil. 1992. Calcium signaling in cell volume regulation. *Physiol. Rev.* 72:1037–1061.

Moura, T.F., R.I. Macey, D.Y. Chien, D. Karan, and H. Santos. 1984. Thermodynamics of all-or-none water channel closure in red cells. *J. Membr. Biol.* 81:105–111.

Price, H.D., and T.E. Thompson. 1969. Properties of lipid bilayers separating two aqueous phases: temperature dependence of water permeability. *J. Mol. Biol.* 41:443–457.

Preston G.M., T.P. Carroll, W.B. Guggino, and P. Agre. 1992. Appearance of water channels in *Xenopus* oocytes expressing red cell CHIP28 protein. *Science (Wash. DC).* 256:385–387.

Rasmusson, R.L., D.G. Davis, and M. Lieberman. 1993. Amino acid loss during volume regulatory decrease in cultured chick heart cells. *Am. J. Physiol.* 264:C136–C145.

Reimer, K.A., and R.B. Jennings. 1992. Myocardial ischemia, hypoxia, and infarction. *In* The Heart and Cardiovascular System. 2nd ed. H.A. Fozzard, E. Haber, R.B. Jennings, A.M. Katz, and H.E. Morgan, editors. Raven Press, New York. 1875–1973.

Reuben, J.P., L. Girardier, and H. Grundfest. 1964. Water transfer and cell structure in isolated crayfish muscle fibers. *J. Gen. Physiol.* 47: 1141–1174.

Rich, G.T., R.I. Sha'afi, A. Romualdez, and A.K. Solomon. 1968. Effect of osmolarity on the hydraulic permeability coefficient of red cells. *J. Gen. Physiol.* 52:941–954.

Rohlicek, A., and A. Schmid. 1994. Dual-frequency method for synchronous measurement of cell capacitance, membrane conductance and access resistance on single cells. *Pflüg. Arch.* 428:30–38.

Sha'afi, R.I., and C.M. Gary-Bobo. 1973. Water and nonelectrolytes permeability in mammalian red cell membranes. *Prog. Biophys. Mol. Biol.* 26:103–146.

Shibata, A., K. Ikawa, T. Shimooka, and H. Terada. 1994. Significant stabilization of the phosphatidylcholine bilayer structure by incorporation of small amounts of cardiolipin. *Biochim. Biophys. Acta.* 1192:71–78.

Solomon, A.K. 1989. Water channels across the red blood cell and other biological membranes. *Methods Enzymol.* 173:192–222.

Sorenson, A.L. 1971. Water permeability of isolated muscle fibers of a marine crab. *J. Gen. Physiol.* 58:287–303.

Stewart, J., and E. Page. 1978. Improved stereological techniques for studying myocardial cell growth: Application to external sarcolemma, T-system and intercalated disks of rabbit and rat heart. *J. Ultrastruct. Res.* 65:119–134.

Suleymanian, M.A., and C.M. Baumgarten. 1994. Cardiac cell volume response to osmotic stress: Temperature-dependence and kinetics. *Biophys. J.* 66:A168.

Tsai, S.-T., R. Zhang, and A.S. Verkman. 1991. High channel-mediated water permeability in rabbit erythrocytes: Characterization in native cells and *Xenopus* oocytes. *Biochemistry.* 30:2087–2092

van Hoek, A.N., and A.S. Verkman. 1992. Functional reconstitution of the isolated erythrocyte water channel CHIP28. *J. Biol. Chem.* 267:18267–18269.

Verkman, A.S. 1993. Water Channels. R.G. Landes Co., Austin. 33–73, 84–97.

Verkman, A.S., and H.E. Ives. 1986. Water transport and fluidity in renal basolateral membranes. *Am. J. Physiol.* 250:F633–F643.

Vieira, F.L., T.I. Sha'afi, and A.K. Solomon. 1970. The state of water in human and dog red cell membranes. *J. Gen. Physiol.* 55:451–466.

Worman, H.J., and M. Field. 1985. Osmotic water permeability of small intestinal brush-border membranes. *J. Membr. Biol.* 87:233–239.

Zadunaisky, J.A., M.N. Parisi, and R. Montoreano. 1963. Effect of antidiuretic hormone on permeability of single muscle fibers. *Nature (Lond.).* 200:365–366.

Zeidel, M.L., S.V. Ambudkar, B.L. Smith, and P. Agre. 1992. Reconstruction of functional water channels in liposomes containing purified red cell CHIP28 protein. *Biochemistry.* 31:7436–7440.

Zheng, J.-S., M.O. Boluyt, Y. Dai, J. Li, X. Long, B.J. Baum, M.T. Crow. 1995. Expression of CHIP28 water channel in aortic-constricted rat heart. *Circulation.* 88:I232.